JOURNAL OF PROPULSION AND POWER
Vol. 15, No. 4, July–August 1999

Analysis of a Hybrid Dual-Combustion-Chamber Solid-Propellant Gas Generator

Jon J. Freesmeier* and P. Barry Butler†
University of Iowa, Iowa City, Iowa 52242

Solid-propellant gas generators (SPGGs) have a number of aerospace applications, including munitions dispersion, pilot emergency escape systems, submarine missile launching, powering actuators and valves, and short-term power supply. Recently, the increased demand for so-called smart automotive airbags has increased the need for SPGG designs capable of real-time, tailorable output. Dual-combustion-chamber gas generators provide several distinct advantages over single-combustor units in systems where optimum performance is needed at several operating conditions. The objective of this work is to evaluate the attainable performance characteristics of a proposed dual-combustion-chamber gas generator. The work includes a simulation of the transient, thermochemical events associated with the firing of an SPGG. The simulations also include the dynamics of coupled events such as ignition, heterogeneous combustion, and mass discharge. The baseline gas generator being simulated in this work is a hybrid SPGG inflator with two combustion chambers. Studies are made of the distribution of propellant between combustion chambers and the times at which the propellant within each combustion chamber is fired.

Nomenclature

A = area, cm^2
a = propellant burning rate prefactor, cm/(s MPa^n)
C_d = discharge coefficient
C_p = constant pressure specific heat, J/g K
C_v = constant volume specific heat, J/g K
d = grain diameter, cm
H = enthalpy, J/g
H_f = enthalpy of formation, J/g
j = computational cell index
k = species index
kk = total number of species
m = mass, g
$\dot{m}$ = mass production rate, g/s
N = number of propellant grains
P = pressure, N/m^2
Q = energy transfer, J
$\dot{Q}$ = energy transfer rate, J/s
R = gas constant, R_u/W, J/g K
R_u = universal gas constant, J/mol K
r = burn depth, cm
T = temperature, K
U = internal energy, J/g
V = volume, cm^3
W = mixture molecular weight, g/mol
W_k = molecular weight of species k, g/mol
Y = mass fraction
γ = specific heat ratio
ΔT = change in temperature (T-298 K), K
ρ = density, g/cm^3
σ = propellant temperature-sensitivity coefficient, K^{-1}
χ = volume fraction of condensed-phase species
ω = gas-phase mass production, g/s

Subscripts

a = chamber A
b = chamber B
c = combustion chamber
eff = effective
gen = generant (propellant)
gr = grain
ign = ignitor
j = cell index
k = species index
P = product
p = plenum
R = reactant
ref = reference state, 298 K, 1 atm
t = discharge tank

Superscripts

cond = condensed phase
gas = gas phase
n = propellant burning-rate pressure index
0 = standard state

Introduction

SOLID-PROPELLANT gas generators (SPGGs) have a number of aerospace applications, including, munitions dispersion, pilot emergency escape systems, submarine missile launching, powering actuators and valves, and short-term power supply.[1] They are also used in road-vehicle, safety-restraint systems,[2] with current installations exceeding 25 million units per year. Industry analysts predict this will increase to 40 million units by the year 2002. Current automotive applications include inflation devices for driver, passenger, and side-impact airbags and knee bolster, and piston actuators for automatic seat-belt tensioners. While the first production-level airbags of the 1960s were inflated by discharging a canister of pressurized gas, SPGGs are now the most common method used to inflate airbags.[2,3] As the main propellant is consumed in an SPGG, hot product gas is formed, which subsequently passes through filters designed to cool the high-temperature gas and remove condensed-phase particulates. The entire deployment process typically takes less than 100 ms for bag inflation devices. In addition to these aerospace and automotive applications, SPGGs are also one of several promising technologies currently being studied as environmentally friendly replacements for Halon-based fire extinguishers.[4] While the technology required to develop and field SPGG fire-suppression devices is not yet fully mature, it has been

Received 3 April 1998; revision received 10 August 1998; accepted for publication 7 October 1998.

*Graduate Research Assistant, Department of Mechanical Engineering; currently at TRW-VSSI, Mesa, AZ.

†Professor, Department of Mechanical Engineering. Associate Fellow AIAA.

demonstrated in full-scale laboratory tests to be effective in extinguishing aircraft gas-turbine engine fires.[4]

Excluding the small percentage of gas produced by the SPGG initiator, most systems currently fielded in automotive and aerospace devices deliver exclusively high-temperature, gaseous combustion products of the condensed-phase propellant. These are referred to herein as pyrotechnic gas generators.[5,6] Over the past decade, the automotive industry has increased the research, development, and production of hybrid gas generators,[7,8] units that discharge a combination of gaseous combustion products and stored, prepressurized, inert gas. Compared with the more conventional pyrotechnic gas generators, hybrid (also referred to as augmented) units generally do not require significant heat removal or special insulating liner materials because they have a lower average gas discharge temperature as a result of the mixing of cold stored gas with hot combustion products. A common link between traditional pyrotechnic and the newer hybrid gas generators is the fact that the discharge process cannot be altered or actively controlled following activation of the igniter. That is, a SPGG burns much like a solid rocket motor with a predetermined burn profile that cannot be modified during operation.

Recently, the increased demand for so-called smart airbags has increased the need for SPGG designs capable of real-time, tailorable output.[9] One method being studied for controllable output is to add a second solid-propellant combustion chamber to a standard hybrid gas generator. Dual-combustion-chamber gas generators provide several distinct advantages over single-combustor units in airbag systems where optimum performance is needed at several operating conditions. The traditional single-combustor gas generator is designed around a single operating state. For example, in the U.S., this is specified as being sufficient to protect an unbelted, 74.5-kg adult in a 48-km/h frontal collision. All other operating conditions are considered off-design. The hybrid, dual-combustion chamber design can be optimized for three operating conditions, and consequently, have more uniform off-design performance. The wider range of acceptable operation is a result of dynamic controllability of the discharge process to match the kinematics of the occupant as they are thrown toward the deploying airbag.

The objective of this work is to evaluate the attainable performance characteristics of a proposed dual-combustion-chamber gas generator. The analysis is performed using Airbag Inflator Model (AIM), a program designed to simulate the transient, thermochemical events associated with the firing of an SPGG.[10] AIM models the processes of gas generation and discharge that are highly nonlinear events governed by first principles, i.e., solving complete conservation equations, variable specific heats, mixture mixing rules, etc. It also includes the dynamics of coupled events such as ignition, heterogeneous combustion, particle filtering, heat transfer, phase change, and mass discharge. Further demands arise when the simulation also requires dual-combustion-chamber configurations for real-time tailorable performance. The SPGG design discussed herein will remain basically the same throughout the study, with small changes made to evaluate the robustness of the design. Typical changes will include changing the distribution of propellant between both combustion chambers, and also, changing the times at which the propellant within each combustion chamber is fired.

Baseline Gas Generator

The baseline gas generator being simulated in this work is a hybrid SPGG inflator with two combustion chambers. It is based on the approximate design specifications of a production-level inflator used to deliver gas to a passenger-side airbag. This unit is configured to pressurize a constant-volume discharge tank to a specified final tank pressure while not exceeding a maximum discharge tank pressurization rate. To achieve these target values, the gas generator must be configured to ignite all propellant at the initial instant of crash detection. The values for maximum discharge tank pressure and pressurization rate are chosen to fall in the middle of the range required for the majority of passenger-side gas generators. For all analyses performed herein, the complete gas-generator system (propellant, gas generator, tank, etc.) is initially at room temperature. To achieve the specified maximum pressure and pressurization rates

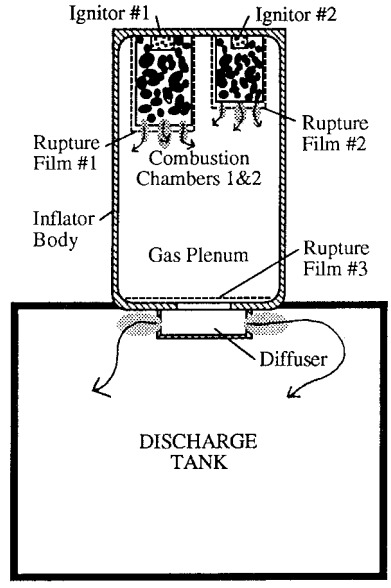

Fig. 1 Cross-sectional view of a typical dual-combustion-chamber augmented passenger-side SPGG airbag inflator.

within the discharge tank, the gas generator discharges a mass of gas into the discharge tank. This gas is a mixture of gas produced from the decomposition of the propellant within the gas generator and the high-pressure, inert gas stored within the gas-generator plenum. A schematic drawing of the gas generator is shown in Fig. 1. The design consists of two sealed combustion chambers contained within a high-pressure plenum. A high-pressure rupture foil initially seals a discharge orifice at the plenum exit. A diffuser is connected to the plenum exit orifice and has exit orifices that are open to the surroundings. Each of the chambers is described in detail in the following sections.

Combustion Chambers

The two combustion chambers within the gas generator are each small in volume, compared with the plenum, and contain the main propellant along with a small amount of igniter propellant. For any gas-generator configuration, the propellant is split between combustion chambers A and B such that total propellant mass is a constant throughout all cases studied in this paper. The propellant mass within each combustion chamber is a combination of both the igniter and main propellant. The mass of propellant in each combustion chamber occupies a portion of the total volume within the combustion chamber. Also, within each combustion chamber is a metallic screen used to capture condensed-phase particulate and to cool the exiting gases. The screen, with a specified mass, is located at the exit of each combustion chamber. The voids within the combustion chambers initially contain a high-pressure inert gas mixture at the same initial pressure and composition as the gas within the gas-generator plenum. Gas can exit each combustion chamber through an array of nozzles, each with individual flow characteristics. The nozzles are initially covered with a burst foil that seals the interior of the combustion chamber from the surrounding plenum. The burst foil is designed to rupture when the pressure within the combustion chamber reaches a predetermined burst pressure.

Gas-Generator Plenum

The gas-generator plenum contains a mixture of inert gas stored at high pressure. The gas-generator plenum has two inlets through which gases can enter the plenum and one exit through which gases are exhausted. The two inlets (the array of exit nozzles from each of the combustion chambers) are identical in size and connect each of the combustion chambers to the plenum. Flow from the combustion chambers into the plenum occurs once the pressure within the combustion chamber exceeds the rupture pressure of the burst foil. At the exit of the gas-generator plenum is a single discharge orifice.

A separate burst foil that is designed to rupture when a specified pressure is reached within the plenum initially covers this opening.

Diffuser

The diffuser is a small chamber connected directly to the exit of the gas-generator plenum. Its purpose is to redirect the gas flow exiting the gas-generator plenum to eliminate axial thrust from the gases exiting the plenum. The diffuser is comparable in volume with the combustion chambers. It has one inlet coming from the gas-generator plenum and has an array of exit nozzles, each equal in size and placed uniformly around the circumference of the diffuser. The exit nozzles of the diffuser are initially open, thus allowing the gas within the diffuser to mix with the gas surrounding the gas generator. The gas initially contained in the diffuser is air at atmospheric conditions.

Discharge Tank

The discharge tank is a constant-volume vessel, where all gas exhausted from the gas generator is collected. It has a volume that is several orders of magnitude larger than the volume of the gas generator and it has no exit nozzles. The only inlet into the discharge tank comes from the exit nozzles of the diffuser. Initially, the discharge tank contains air at atmospheric conditions. The dominant pathway for heat transfer within the discharge tank is assumed to occur between the gas within the discharge tank and the discharge tank wall.

Propellant Formulation

The propellant used throughout this study is a polyvinyl chloride (PVC) and potassium perchlorate (KP) formulation, with small amounts of several binders and minor constituents. The enthalpy of formation of this propellant mixture is calculated to be −3280 kJ/kg and the mixture density is 2.08 g/cc. It is assumed the combustion process proceeds at an equilibrium state during the complete burning process of the propellant. It is also assumed that surrounding conditions do not deviate substantially during the combustion process. Therefore, the distribution of product species calculated at one flame state are assumed to be the same throughout the combustion process.[7] With these assumptions, an adiabatic flame temperature calculation can be performed at an estimated average pressure within the combustion chamber.

The standard JANNAF[11] species database was used for calculating the thermochemical properties of the products of combustion for the propellant. Product species were chosen from this database by minimizing the Gibb's free energy of the reacting system within a specified tolerance while satisfying the elemental population constraint. Propellant Equilibrium Program (PEP)[12] a thermochemical equilibrium calculation program, was used to solve the system of equations to determine the adiabatic flame temperature and the relative amounts of product species. The average combustion pressure was estimated to be 20.6 MPa. At this pressure, the adiabatic flame temperature was calculated to be 2898 K with the major equilibrium products shown in Table 1. From Table 1, it can be seen that all product species are in the gaseous phase. With no condensed-phase products present, the filter screens within the gas generator act only as heat sinks for the hot combustion gases and not as mass-collection devices. Also from Table 1, it is observed that the species H_2O, CO_2, KCl, and K_2Cl_2 account for 90% of the mass of gaseous products. At the pressures and temperatures seen within the gas generator, it is noted that the product species H_2O and KCl are close to their respective vaporization/condensation lines. Thus, under some operating conditions, they have the potential to condense during the expansion process to form liquid.

Table 1 Equilibrium products of combustion for KP PVC propellant composition[a]

Species	Phase	Molecular weight	Mole %	Mass %
H_2O	Gas	18.01	27.094	10.632
CO	Gas	28.01	1.462	0.892
CO_2	Gas	44.01	34.666	33.230
HCl	Gas	36.46	3.066	2.435
O_2	Gas	32.00	6.427	4.479
K_2Cl_2	Gas	149.11	3.710	12.048
OH	Gas	17.01	1.137	0.421
KCl	Gas	74.56	21.003	34.107
KOH	Gas	56.11	1.437	1.756

[a]At adiabatic flame conditions at $P = 20.6$ MPa g (3000 psig).

Ballistic Model

Several fundamental assumptions are made in deriving the governing equations for analyzing an SPGG. These assumptions apply to all gas-generator models discussed in this study and are shown along with justification in the following:

1) Gas- and condensed-phase components are composed of multiple species with temperature-dependent specific heats. Justification: the gas- and condensed-phase products are present over a wide range of temperatures (300−3000 K), thus requiring the specific heats to be evaluated as functions of temperature.

2) The gas-phase species are well mixed (spatially uniform) within each computational cell, and the properties of gas exiting a cell are the same as the gas accumulated in the cell. Justification: for the present design, extreme turbulent mixing occurs during the discharge process, resulting in fluid mixing time scales much smaller than diffusional time scales.

3) Propellant decomposition is restricted to the combustion chambers. Gas-phase reactions can occur in all cells. Justification: SPGG systems are typically designed so that the unreacted solid propellant is restricted to a well-defined combustion chamber through the use of a filtering screen. However, gas-phase chemical reactions can occur in other locations, where fuel and oxidizer species are present at appropriate concentrations and temperature. Some SPGG systems are designed to permit secondary gas-phase burning in the plenum volume.[7]

4) Ignition of the propellant grains occurs at a user-defined ignition delay time. Justification: propellant ignition is a complex process involving several dependent parameters difficult to quantify; thus an empirical expression was determined from experimental data.

5) All hardware items and metallic filter/cooling screens are treated as nonadiabatic, energy-absorbing components with time-varying temperatures. Justification: in some SPGG systems, heat transfer to hardware and filter components can account for a significant amount of the total energy available from decomposition of the propellant.

Based on these assumptions, the conservation equations for the various gas-generator systems are derived by applying conservation principles of mass and energy to each volumetric cell within the system. From this derivation, a system of ordinary differential equations (ODEs) is developed to express the time derivatives of all dependent variables: gas- and condensed-phase temperatures within each cell, hardware temperatures, and individual species mass within each cell. These differential equations combine with the constitutive relations to form the governing equations for the gas-generator systems.

Thermodynamic Data

Individual gas- and condensed-phase chemical species are tracked throughout the numerical simulation, thus requiring thermodynamic properties for each chemical species over a wide range of conditions. A fourth-order polynomial expansion in temperature is used to represent the standard-state, constant-pressure specific heat data for the individual species $C^0_{p,k}(T)$. Standard-state enthalpy of the species can be determined by the fundamental thermodynamic relationship

$$H^0_k(T) = \int_{T_{\text{ref}}}^{T} C^0_{p,k}(T) + H^0_{f,k}(T_{\text{ref}}) \tag{1}$$

Equation of State

All condensed-phase species are considered incompressible:

$$\rho_{\text{cond},j} = \text{const} \tag{2}$$

whereas the ideal gas equation of state is used throughout the gas-generator model to represent the pressure–volume–temperature relationship between the gas-phase species present within the jth volumetric cell:

$$P_j = \rho_j R_j T_j \tag{3}$$

where R_j, the gas constant for cell j, is dependent on the local mixture molecular weight $W_j = \Sigma X_k W_k$.

Conservation Equations

Using the basic model assumptions listed in the preceding text, the conservation equations of species mass and energy are applied to the individual volumetric cells within a gas-generator system. The computational network shown in Fig. 2 represents the gas-generator system discussed previously. Within this network, each cell is designated with the index j, whereas the upstream and downstream cells are identified as $j-1$ and $j+1$, respectively. The gas within the volumetric cell j of size V_j is well mixed (spatially uniform), and has properties P_j, T_j, and ρ_j. The mass inflow from cell $j-1$ is uniform across the inlet area, and has properties P_{j-1}, T_{j-1}, and H_{j-1}, where H_{j-1} is the enthalpy of the mixture in cell $j-1$. Figure 2 shows enlarged views of both the combustion chamber (cell $j =$ 1B) and the high-pressure plenum (cell $j = 2$).

For each control volume j depicted in Fig. 2, species conservation can be stated in differential form as

$$\frac{\mathrm{d}m_{k,j}}{\mathrm{d}t} = Y_{k,j-1}\dot{m}_{j-1} - Y_{k,j}\dot{m}_j + \dot{\omega}_{k,j} + \dot{m}_{\mathrm{gen},k,j} \tag{4}$$

The sum of $\dot{\omega}_{k,j}$, the gas-phase mass production rate, and $\dot{m}_{\mathrm{gen},k,j}$, the mass addition caused by propellant decomposition, represent the rate of mass production within the control volume, and Y_k is the mass fraction for species k.

For the individual control volumes shown in Fig. 1, the model assumptions are applied and the conservation of energy for the gas mixture is written in differential form as

$$\frac{\mathrm{d}T_j^{\mathrm{gas}}}{\mathrm{d}t} = \frac{1}{m_j^{\mathrm{gas}} C_{vj}^{\mathrm{gas}}}\left[\sum_{k=1}^{kk}(U_{k,j}\dot{\omega}_{k,j}) + H_{j-1}^{\mathrm{gas}}\dot{m}_{j-1}^{\mathrm{gas}} - H_j^{\mathrm{gas}}\dot{m}_j^{\mathrm{gas}} + \dot{Q}_j^{\mathrm{gas}} + H_j^{\mathrm{gas}}\dot{m}_{\mathrm{gen,j}}^{\mathrm{gas}} + P_j V_j^{\mathrm{gas}}\frac{\mathrm{d}\chi_j}{\mathrm{d}t}\right] \tag{5}$$

The production of gas from a burning propellant is dependent on the propellant surface regression rate $\dot{r}_{\mathrm{gr}}$, instantaneous propellant grain surface area A_{gr}, and propellant density ρ_{prop}. The propellant burning rate is modeled as a function of pressure and variation from ambient temperature ΔT, and is represented by the form[13]

$$\dot{r}_{\mathrm{gr}} = a e^{\sigma \Delta T} P^n \tag{6}$$

Here, r_{gr} is the burn depth measured from the initial surface of the propellant. Equation (6) is a typical burn-rate function for propellants under quasi-steady-state pressure conditions. The variation of the propellant grain surface area, on which a flame is propagating, with burn depth is primarily dependent on the geometry of the propellant grain as well as flame-spreading characteristics, and can also change because of grain fracture. For this study, it is assumed that the form function is only a function of grain geometry. Thus, it is assumed that flame spread is instantaneous on the grain surface at the time of ignition and no grain fracture occurs. Analyzing the regression of the propellant grain shape can easily develop a form function based solely on geometry. For all results presented herein, the propellant grains are modeled as solid right circular cylinders, initially 0.4 cm in length and 1.5 cm in diameter, which burn uniformly on all exposed surfaces. The right-circular cylinder geometric shape provides a well-defined mathematical relationship between the surface area of the propellant grain and the burn depth. The right-circular cylinder geometric shape produces an initial surface area per grain of 5.42 cm^2.

The total rate of mass addition to the system caused by propellant decomposition is

$$\dot{m}_{\mathrm{prop}} = N_{\mathrm{gr}} A_{\mathrm{gr}} \rho_{\mathrm{prop}} \dot{r}_{\mathrm{gr}} \tag{7}$$

Combining the rates of mass production rate from the propellant and igniter charge according to

$$\dot{m}_{\mathrm{gen}} = \dot{m}_{\mathrm{ign}} + \dot{m}_{\mathrm{prop}} \tag{8}$$

provides closure for the addition of mass to the system, and completes the necessary relations to conserve mass within the gas-generator system.

The mass flow exiting each volumetric cell through the local nozzles is classified as either in the sonic or subsonic flow regime, depending on the pressure difference between the adjacent cells and the specific heat ratio of the gaseous mixture within the volumetric cell from which the gases are exiting. The choked flow critical condition is calculated to determine whether a sonic or subsonic flow condition exists for the mass flow between two cells using the preceding parameters. Applying the fundamental laws of gasdynamics, the gas-phase mass flow rate is determined from the following sonic and subsonic relations.

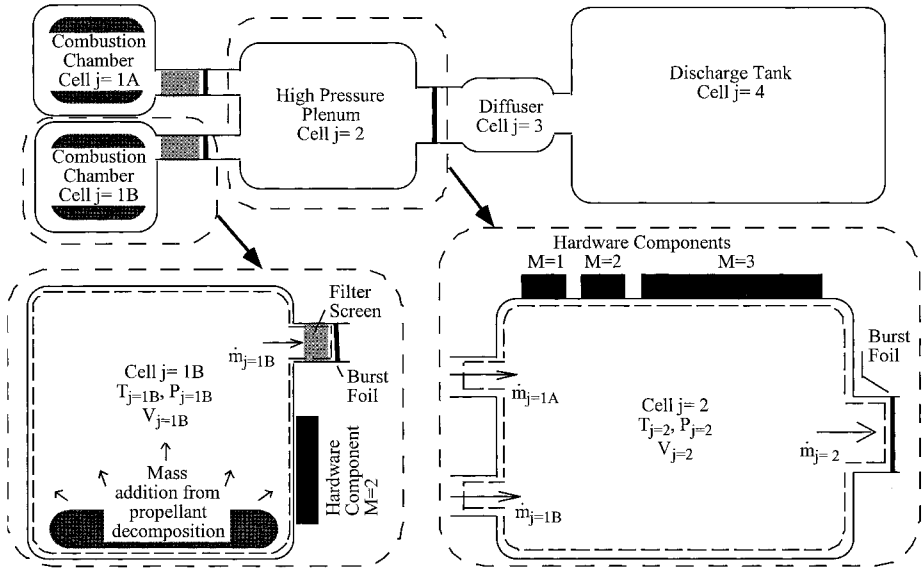

Fig. 2 Computational network for the inflator system with expanded views of combustion chamber B and the high-pressure plenum.

Subsonic:

$$\dot{m}^{\text{gas}} = A_{\text{flow}} C_d \sqrt{\frac{2\gamma}{\gamma - 1} P_{+\rho+} \left[\left(\frac{P_+}{P_-} \right)^{2/\gamma} - \left(\frac{P_+}{P_-} \right)^{(\gamma+1)/\gamma} \right]} \tag{9}$$

Sonic:

$$\dot{m}^{\text{gas}} = A_{\text{flow}} C_d \sqrt{\gamma P_{+\rho+}} [2/(\gamma + 1)]^{[(\gamma+1)/[2(\gamma-1)]]} \tag{10}$$

In Eqs. (9) and (10), A_{flow} and C_d are the respective flow area and discharge coefficient for the given nozzle.[14] The subscripts + refers to the high-pressure chamber, and − refers to the low-pressure chamber. All heat transfer calculations within the gas-generator model system are based on an effective heat transfer coefficient, h_{eff}, which incorporates the three modes of heat transfer, conduction, convection, and radiation, into one term.

Results

The generic gas-generator configuration described previously is used to evaluate the performance of a dual-combustion-chamber gas generator. With knowledge of the basic performance requirements for a passenger-side gas generator, a baseline configuration was defined. Tables 2 and 3 provide a complete description of all the parameters specified for the baseline gas-generator configuration. From this baseline configuration, changes were subsequently made to access the capability of the particular style of gas generator to meet the requirements for a tailorable gas generator used in smart airbag systems.

Inflator Performance Parameters

When testing SPGGs, it is important to gather enough information to determine if it will perform as expected in a specific application. To determine the performance of an inflator, both the initial conditions and the thermodynamic states of various subcomponents during the transient process must be known. To speed testing times and obtain reproducible data, SPGG inflators are typically tested by firing into a constant volume discharge tank. This process has become the industry test standard. It is desirable because it enables technicians to permanently instrument a test vessel to obtain the necessary property data for thousands of firings required for certification. By firing the inflator in a constant-volume discharge tank as a validation, it is necessary to develop a correlation between the tank data taken from a discharge tank and expected performance in a fielded application.

Tank pressure and temperature are the typical measurements taken during the discharge of an airbag inflator. With pressure and temperature histories in a chamber and knowledge of the chemical composition, many additional properties can be found, including mass-flow rates. By knowing the pressure and temperature histories within a chamber, both the differentials (pressure-rise rates) and time integrals (impulse values) can also be determined. With these properties of the inflator system known, an accurate determination of the inflator performance can be made. The following is a description of several key parameters used in the determination of inflator performance.

The pressure history in the inflator plenum plays a significant role in determining several operating characteristics of the SPGG inflator, including 1) times at which burst foils rupture, and 2) flow characteristics between chambers. The most important information gathered from the pressure histories is the peak pressure within each chamber internal to the inflator. This pressure is essential in assessing the potential for catastrophic structural failure of the inflator. Depending on the size and shape of the inflator body, the maximum allowable peak pressure can vary dramatically. However, typical peak pressures for airbag SPGG inflators are in the range of 50–60 MPa (7248–8698 psig).

The temperature history is also important in determining the reliable performance of an inflator. Temperatures within an inflator can potentially reach up to 2000 K in localized areas. The dynamic events associated with the discharge of an airbag inflator, including the high-velocity discharging of combustion product gases, can lead to hot areas within an inflator. This can affect the performance of the inflator by potentially increasing or decreasing nozzle size by removing or depositing metal in the nozzle vicinity. Knowing the gas temperature within the inflator can help determine if localized hot spots will reach a high enough temperature to cause hardware melting. The temperature histories also help determine other operational characteristics of the inflator such as mass-flow rates.

Table 2 Inflator baseline configuration: generic characteristics

Name	Identification number	Volume	Pressure	Temperature	Gas composition mass fraction	Propellant mass, g
Combustion chamber 1A	1A	20 cm^3 (1.2 in.^{3})	27.7 MPa g (4013 psig)	298 K 77°F	Ar = 0.95 He = 0.05	12.3
Combustion chamber 1B	1B	20 cm^3 (1.2 in.^{3})	27.7 MPa g (4013 psig)	298 K 77°F	Ar = 0.95 He = 0.05	12.3
High-pressure plenum	2	337 cm^3 (20.5 in.^{3})	27.7 MPa g (4013 psig)	298 K 77°F	Ar = 0.95 He = 0.05	——
Diffuser	3	25 cm^3 (1.5 in.^{3})	0.0 kPa g (0.0 psig)	298 K 77°F	O_2 = 0.21 N_2 = 0.79	——
Discharge tank	4	60,000 cm^3 (3661 in.^{3})	0.0 kPa g (0.0 psig)	298 K 77°F	Ar = 0.95 He = 0.05	——

Table 3 Inflator baseline configuration: flow characteristics

Name	Identification number	Total nozzles	Total nozzle area	Nozzle diameters	Discharge coefficient	Opening criteria
Combustion chamber 1A	1A	12	202.9 mm^2 (0.314 in.^{2})	4 @ 7.35 mm 8 @ 2.30 mm	0.9 0.9	$P_{c,a}$ = 28.3 MPa g
Combustion chamber 1B	1B	12	202.9 mm^2 (0.314 in.^{2})	4 @ 7.35 mm 8 @ 2.30 mm	0.9 0.9	$P_{c,b}$ = 28.3 MPa g
High-pressure plenum	2	1	56.7 mm^2 (0.088 in.^{2})	1 @ 8.50 mm	1.0	P_p = 45.5 MPa g
Diffuser	3	10	384.8 mm^2 (0.596 in.^{2})	10 @ 7.00 mm	0.65	Open initially
Discharge tank	4	0	0	0	0	N/A

The pressure profile within the discharge tank has been historically one of the most important parameters used in determining the performance of an individual inflator. The pressure history contains several pieces of key information used to evaluate the inflator. For a passenger-side inflator, an average peak tank pressure is 660 kPa g in a 60-l discharge tank, whereas an average driver-side inflator will produce a 220 kPa g peak pressure within the same discharge tank.

Also of interest from the discharge tank pressure profile is the time of the initially detected pressure rise within the discharge tank. This time tells how quickly an inflator can begin to discharge gas into an airbag after it receives a signal from the crash sensors. Most driver- and passenger-side airbags need to have the time of first pressure rise to be within 5−10 ms of crash detection. For side-impact airbags, this time must be much shorter, in the range of 3−5 ms because of the reduced distance between impact and occupant.

The pressure-rise rate within the discharge tank is another very important performance indicator. This indicator shows how fast that a particular inflator can discharge gas into the airbag. The pressure-rise rate within the discharge tank is not an independently measured quantity, but instead comes from the first differential of the measured pressure history. A faster pressure-rise rate does not necessarily imply a better inflator design. Typically, for passenger-side inflators, a pressure-rise rate between 16 and 20 kPa/ms (2.3 and 2.9 psi/ms) is desired. For a driver-side inflator, pressure-rise rates vary between 10 and 14 kPa/ms (1.4 and 2.0 psi/ms). A pressure-rise rate that is too low results in a situation where not enough gas is discharged into the airbag quickly enough, and inadequate protection is given by the airbag. If the pressure-rise rate is too large, the gases are discharged too quickly, resulting in an airbag that is too stiff to provide a cushioning effect in a crash and could potentially lead to additional injuries caused by the airbag deployment. Typically, the pressure-rise rate is measured over the time period from when gas first enters the discharge tank to $\sim t = 40$ ms. This is the time period when the bag inflates and initial interaction between the occupant and the airbag occurs. After this time the pressure-rise rate falls and approaches zero as the discharge of gas is completed.

Because the pressure-rise rate is the first differential of the pressure history, it must be determined directly from the pressure history. This leads to several different methods for calculating the pressure-rise rate. The instantaneous and 5-ms window-averaged curves are two different ways of presenting the information concerning the pressure-rise rate within the discharge tank. Both representations have distinct advantages and disadvantages in describing the pressure rise in the discharge tank.

The instantaneous pressure-rise rate is calculated by finding the slope of a line between two sequential pressure measurements. This method works well for determining exactly when certain processes occur, but also has a tendency to amplify any noise associated with the individual measurements. The instantaneous curve shows the true time when gas within the inflator begins to enter the discharge tank, but also exhibits a large amount of noise at higher pressurization rates, which complicates determining the maximum pressure-rise rate and the time at which it occurs.

A second method, used more in industry, is the 5-ms window-averaged curve. This method also has its merits. The 5-ms window-averaged curve, as its name suggests, requires a 5-ms window of pressure measurements to determine the appropriate slope of the line. All pressure measurements with the 5-ms window are used to obtain a linear best-fit line, using the method of least squares, through the data points. The pressure-rise rate at the midpoint of the 5-ms window is then assigned the value of the slope of the best-fit line over the 5-ms time period. After this is completed, the 5-ms window is shifted by including the next pressure measurement and removing the first pressure measurement from the 5-ms series. This method, while eliminating the noise of the instantaneous curve, shortens the time between the inflator firing and the initial pressure rise within the discharge tank. Throughout the remainder of this paper, the 5-ms window-averaged method will be used to present the pressure-rise rate in a volumetric chamber.

Gas-Generator Description Nomenclature

Throughout the remaining discussion, the results from the various configurations of the baseline gas-generator model will be distinguished by the nomenclature XX(a)/YY(b). Here, XX represents the mass percentage of main propellant contained within combustion chamber A ($m_{p,a}/m_p$), and YY represents the mass percentage of main propellant contained within combustion chamber B. The sum of XX and YY is always 100. The variables (a) and (b) represent the ignition delay time in milliseconds for the respective combustion chambers. Because at least one of the combustion chambers is always fired at $t = 0$ ms, the value of either (a) or (b) will be zero. For all cases, the variable (a) or (b) that has a value of zero will be eliminated from the notation, thus shortening the notation. For example, XX(a)/YY implies chamber B fires at $t = 0$ ms, whereas XX/YY(b) indicates chamber A fires at $t = 0$ ms. Finally, for some configurations, either combustion chamber A or B is not fired, resulting in an infinite value for (a) or (b). For this condition, the appropriate variable, (a) or (b), is assigned the character notation nf, short for never fired. This notation is meant to indicate the firing sequence as well as differentiate the multiple options available for a single configuration of a dual-combustion-chamber gas generator. As previously discussed, a single configuration is where only the distribution of main propellant is predetermined; thus the combustion chamber firing sequence and delay times remain variable, resulting in a vast array of performance characteristics.

There are two primary sets of firing options possible for a dual-combustion-chamber gas generator. The first is firing either a single or both combustion chambers at the beginning of the simulation. These firing options can be grouped together by the fact that the output of the gas generator is determined solely at the beginning of the process. That is, no additional changes are made to the operation of the gas generator after the initial firing of the gas generator. The second firing option is characterized by firing of a single-combustion chamber initially, whereas the second combustion chamber is not fired until a specified delay time is exceeded. This set of options is grouped together by the fact that operation of the gas generator is determined at the beginning of the simulation, but is also affected by additional inputs occurring at the specified delay times. This second set of firing options requires sensor equipment that is more complex because of the delay times between firing the individual combustion chambers. This set of firing options will be the focus of this study. The firing options for the dual-combustion-chamber gas generator previously discussed will focus on firing combustion chamber A at $t = 0$ ms, and then firing combustion chamber B at a finite delay time $t_{\text{ign},b}$. The delay times studied are $t_{\text{ign},b} =$ 0, 5, 10, and 20 ms.

Test Configurations

To determine the effect of specifying a delay time between combustion chamber firings, it is necessary to have propellant distributions that perform similarly by firing only chamber A at $t = 0$ ms. The propellant distributions studied here in are $\frac{50}{50}$, $\frac{60}{40}$, and $\frac{80}{20}$, where the larger percentage of propellant is contained within combustion chamber A, and combustion chamber A is always fired at $t = 0$ ms. Combustion chamber B is then fired at a specified delay time of $t_{\text{ign},b} =$ 0, 5, 10, 15, and 20 ms. The purpose of this discussion is to describe the variations in performance characteristics of the gas generator caused by changes in the firing time of the second combustion chamber.

Plenum and Discharge Tank Performance Curves

Pressure and temperature histories within the gas-generator plenum and discharge tank will be used to assess the differences between delay times for firing combustion chamber B. The pressure rise rate within the discharge tank will also be used to differentiate between firing scenarios. Figures 3 and 4 show the pressure history within the gas-generator plenum for 50/50 and 80/20 propellant distributions, respectively. In each figure, pressure histories are shown for four delay times ($t =$ 0, 5, 10, 15, and 20 ms). It can be seen that, with a delay time of $t_{\text{ign},b} = 0$ ms, the plenum pressure history for each propellant distribution is the same. These results are expected because all propellant contained within the gas generator is fired at $t = 0$ ms for all scenarios described. The pressure histories shown in Figs. 3 and 4 can be divided into three distinct regions: 1) the time between firing combustion chamber A ($t_{\text{ign},a} = 0$ ms) and the time at which the gas-generator plenum burst foil ruptures ($5 < t < 10$ ms);

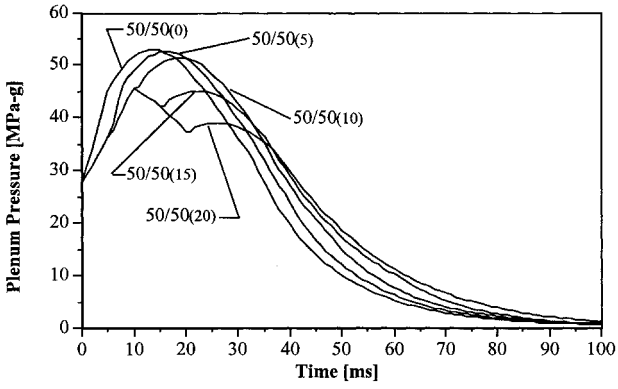

Fig. 3 Inflator plenum pressure histories for five different delay firing times of an inflator configuration with $\frac{50}{50}$ propellant distribution.

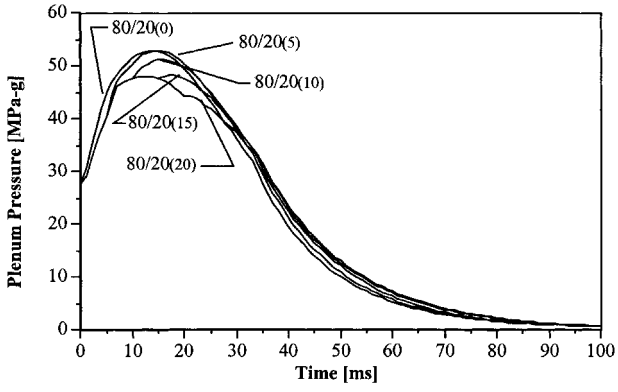

Fig. 4 Inflator plenum pressure histories for five different delay firing times of an inflator configuration with $\frac{80}{20}$ propellant distribution.

2) the time between the rupturing of the gas-generator plenum burst foil and the time when all propellant is consumed ($34 < t < 40$ ms); and 3) the time after the propellant is completely consumed to when the expansion process within the gas generator is completed.

The first region, the time between firing combustion chamber A and when the gas-generator plenum burst foil is ruptured, is identified by a nearly linear increase in pressure within the gas-generator plenum. The rate of pressure increase in this region is determined by the amount of propellant burning during this time. As expected, the cases where 80% of the propellant is ignited at $t_{\text{ign},a} = 0$ ms have a greater initial pressure-rise rate than the cases where 50% of the propellant is ignited at $t_{\text{ign},a} = 0$ ms. For both propellant distributions, $\frac{50}{50}$ and $\frac{80}{20}$, rupturing of the gas-generator plenum burst foil occurs before the ignition of combustion chamber B, except for delay times of $t_{\text{ign},b} = 0$ and 5 ms. This result is obvious for the delay time of $t_{\text{ign},b} = 0$ ms, but for the delay time of $t_{\text{ign},b} = 5$ ms, it is noted by an increase in the pressure rise between 5 ms and the time of burst foil rupturing in the gas-generator plenum.

The second region, the time between plenum burst foil rupturing and the consumption of all propellant within the gas generator, is the region where the most noticeable differences occur between the various firing delay times and propellant distributions. The starting point of this region is noted by a sudden change in the pressure-rise rate. This is caused by the sudden discharge of gas through the exit nozzle of the gas-generator plenum. In this region, the combination of mass addition from the decomposition of the propellant and the discharge of gas through the exit nozzles determines whether the pressure will continue to rise within the gas-generator plenum. For the $\frac{50}{50}$ gas-generator configuration, the delay time for firing combustion chamber B is the most influential parameter in determining whether the pressure will continue to rise or begin declining within the gas-generator plenum. In these configurations, the delay times of $t = 15$ and 20 ms are long enough after the opening of the plenum exit nozzles for the pressure to begin decreasing within the gas generator plenum. The amount of the pressure decrease is proportional to the increase in the delay time of firing combustion chamber B. For all cases with the previously mentioned propellant distributions, the firing of combustion chamber B at the specified delay time is signified by an almost immediate increasing pressure within the gas-generator plenum. For the $\frac{80}{20}$ gas-generator configuration, the delay time parameter has less of an effect on the pressure rise or decrease within the gas-generator plenum. For all delay times studied here, the pressure continues to increase after the plenum exit nozzle opens. This is because of the large amount of propellant still burning in combustion chamber A. The trends seen in the $\frac{80}{20}$ configuration still follow the trends seen in the $\frac{50}{50}$ configuration, except to a lesser degree.

The end of the second region is signified by the complete consumption of all propellant within the gas generator. In Figs. 3 and 4, this point is noted by a distinct change in the rate of pressure decrease within the gas-generator plenum. For all configurations and delay times, this change occurs between $t = 35$ and 40 ms. It is important to note the minimal effect of the delay time parameter on the burnout time of the propellant. With delay times of $t = 0$–20 ms, the burnout of the propellant still occurs within 5 ms for all firings.

The third region, the time after complete propellant burnout, is a time where the gas-flow dynamics are governed by the laws of a polytropic expansion process. The difference in the decrease in plenum pressure between various firing conditions is determined solely by the conditions within the gas-generator plenum at the time of propellant burnout. This process proceeds until equilibrium between the gas-generator plenum and discharge tank is reached. Although it appears from Figs. 3 and 4 that significantly different performance occurs between various delay times for a gas generator, it is important to evaluate the performance changes occurring external to the gas generator. It is important to determine whether the different internal performance characteristics lead to any substantial changes to discharge tank performance. Figures 5 and 6 show the pressure histories predicted within the discharge tank for the propellant distributions and delay times shown in the previous figures.

Figures 5 and 6 demonstrate that all discharge tank pressure histories follow the same general trend, whereas small differences occur between propellant distributions and delay times. The most noticeable is the change in performance because of a change in the specified delay time. An increase in the delay time specified for firing combustion chamber B results in a decrease in the rate of pressurization (slope of the pressure history) within the discharge tank. While the rate of pressurization is altered by the change in delay times, the time at which pressure begins to increase within the discharge tank (the time gas begins to enter the discharge tank from the gas generator) is not significantly changed. Also, the peak pressure predicted within the discharge tank is not significantly altered by the change in delay time.

A comparison between pressure histories for the two propellant distributions shows results more closely related for the $\frac{80}{20}$

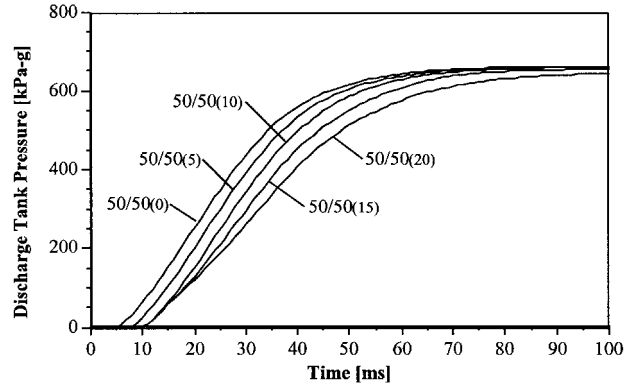

Fig. 5 Discharge tank pressure histories for five different delay firing times of an inflator configuration with $\frac{50}{50}$ propellant distribution.

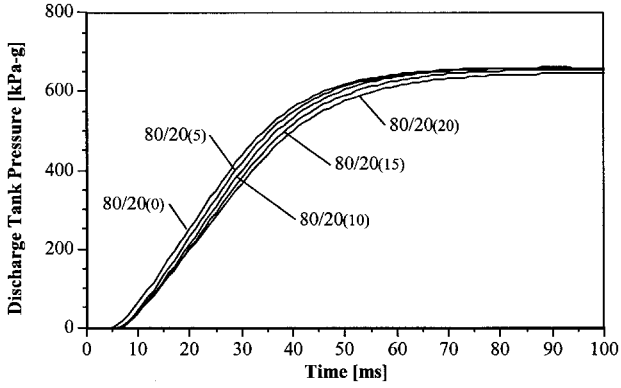

Fig. 6 Discharge tank pressure histories for five different delay firing times of an inflator configuration with $\frac{80}{20}$ propellant distribution.

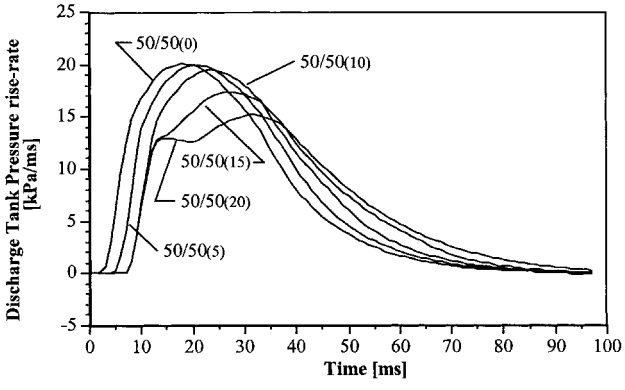

Fig. 7 Discharge tank 5-ms window-averaged, pressure-rise rates for five different delay firing times of an inflator configuration with $\frac{50}{50}$ propellant distribution.

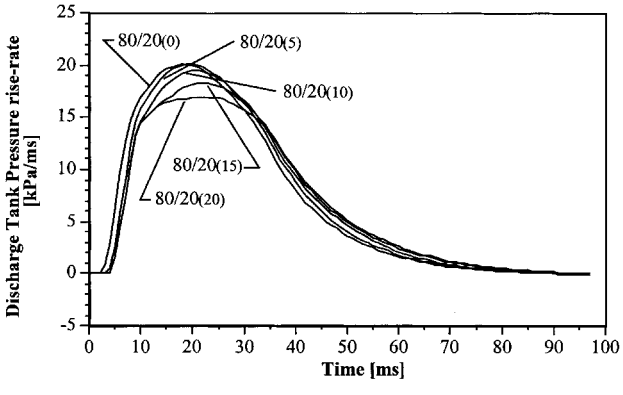

Fig. 8 Discharge tank 5-ms window-averaged, pressure-rise rates for five different delay firing times of an inflator configuration with $\frac{80}{20}$ propellant distribution.

distribution and growing wider, moving to the $\frac{50}{50}$ distributions. This can be accounted for by the large amount of propellant ignited initially in the $\frac{80}{20}$ distribution. With this distribution, only 20% of the propellant remains to be ignited in combustion chamber B after the delay. While this is a significant amount, it does not provide enough mass generation to drastically alter the pressure history characteristics within the discharge tank. On the other hand, the $\frac{50}{50}$ distribution ignites much less propellant initially and has a larger amount of propellant to be ignited within combustion chamber B. This results in a wider variation of performance characteristics within the gas generator as well as in the discharge tank.

Figures 7 and 8 are included to show the 5-ms, window-averaged, pressure-rise rate within the discharge tank. Here, the same general trends between propellant distributions occur for each delay time specified. During approximately the first 5 ms after the opening of the nozzles at the exit of the inflator plenum, the pressure-rise rate increases nearly the same for all delay times, and propellant distributions indicating the behavior during this time is heavily dependent on the inflator burst foil rupture pressure. After the first 5 ms, the effect of the delay time parameter becomes noticeable. The shorter delay times of $t = 0, 5$, and 10 ms produce pressure-rise rates curves similar to those produced by single combustion chamber inflators, i.e., a rounded peak relatively early in the scenario with a steady decline following. The delay times of $t_{\text{ign},b} = 15$ and 20 ms begin to show a plateau effect in the region where the shorter delay times produce a definite peak in pressure rise. This plateau, although lower in magnitude, lasts approximately the same time as it takes other curves to rise to their respective peak values and return to the same value as the plateau curve. The resulting decrease in pressure-rise rate for the plateau curve is much less than the decline of the curves that achieved a definite peak value.

Figure 9 compares the range of achievable maximum pressure-rise rates from various delay times for a range of propellant distributions. It presents the pressure-rise rate within the discharge tank at $t = 10$ ms (solid line) and $t = 20$ ms (dashed line), while varying both the propellant distribution between combustion chambers and the firing delay time $t_{\text{ign},b}$. The results are limited to propellant mass ratios ($m_{p,a}/m_p$) between 0.5 and 0.8. Below this range, the gas generator would not meet some of the predetermined requirements, i.e., gas flow into the discharge tank under 10 ms, for the operation of the gas generator. Above $m_{p,a}/m_p = 0.8$, the operation of the gas generator becomes almost uniform with changing $m_{p,a}/m_p$ ratios; thus these ratios are also not of interest. From Fig. 9, it can be seen that the pressure rise is always greater at $t = 20$ ms than at $t = 10$ ms, but the magnitude of difference is greater with even

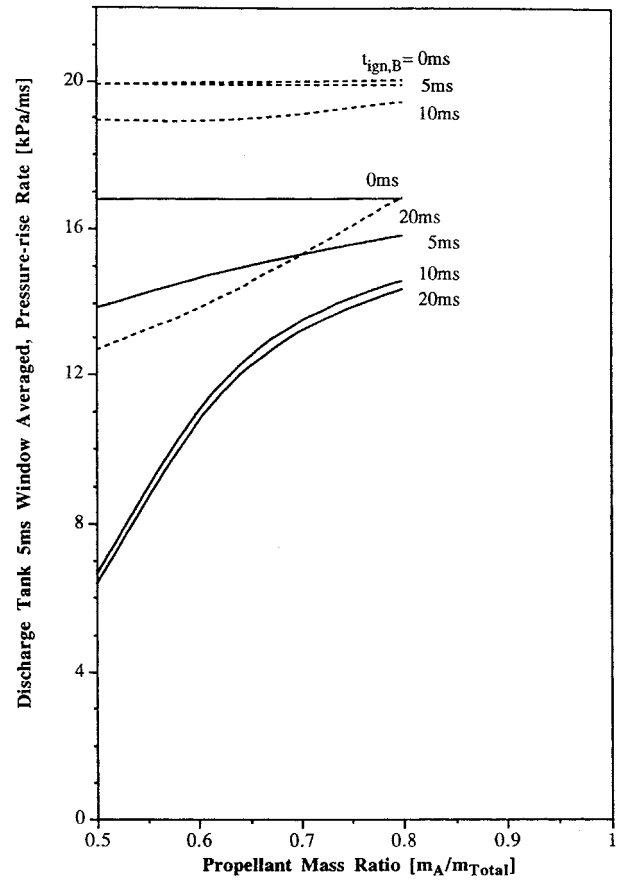

Fig. 9 Discharge tank 5-ms window-averaged, pressure-rise rates evaluated at t = 10 (solid lines) and 20 ms (dashed lines) for $t_{\text{ign},b}$ = 0, 5, 10, and 20 ms.

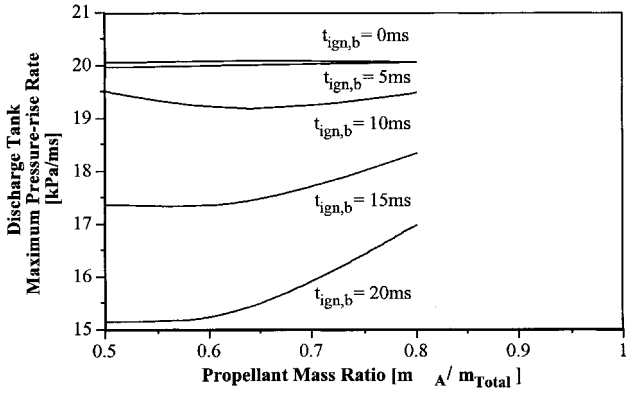

Fig. 10 Discharge tank 5-ms window-averaged, maximum pressure-rise rates for $t_{ign,b} \leq 20$ ms at several propellant mass ratios.

propellant distributions ($m_{p,a}/m_p = 0.5$) than with uneven distributions ($m_{p,a}/m_p = 0.8$). Also, from Fig. 9, it can be noted that the pressure-rise rate at $t = 10$ ms is affected to a greater extent by the delay firing time of combustion chamber B ($t_{ign,b}$) than is the pressure-rise rate at $t = 20$ ms, particularly when $t_{ign,b}$ is 10 ms or less. Figure 9 demonstrates how the gas-generator configurations with well-balanced propellant distributions, i.e., $m_{p,a}/m_p = 0.5$, can produce tank curves with a wider range of maximum pressure-rise rates than those with uneven propellant distributions given a range of allowable delay times for igniting combustion chamber B.

Figure 10 complements Fig. 9 by showing the maximum pressure-rise rate within the discharge tank, while again varying the propellant distribution between combustion chambers and the firing delay time $t_{ign,b}$. The trends occurring in Fig. 10 are similar to those occurring in Fig. 9, i.e., the pressure-rise rate for each firing delay time begins to approach $t_{ign,b} = 0$ ms as the propellant mass ratio approaches 1.

Conclusions

The so-called smart SPGG analyzed herein is capable of delivering a range of output characteristics. The results presented here are intended to show the possible performance trends for this type of SPGG system. Trends predicted by an SPGG simulation model (AIM) show a minimum of 45% of the total solid propellant mass must be fired at $t = 0$ ms to produce an increase in tank pressure within 10 ms, a desirable performance characteristic for next-generation airbag inflators. The model also predicts that all propellant distributions with 45% or more of the solid propellant fired at $t = 0$ ms produce acceptable output characteristics, assuming the second combustion chamber is fired within 20 ms. Furthermore, the peak pressure within the discharge tank is minimally affected by the propellant distribution or ignition delay time of the second combustion chamber. Conversely, the time of first gas flowing into the discharge tank and pressure-rise rate history within the discharge tank are parameters affected most notably. Short delay firing times ($t_{ign,b} = 0$–10 ms) produce performance characteristics with output closely following the limiting condition, where 100% of the propellant is fired at $t = 0$ ms. Large delay firing times studied ($t_{ign,b} =$ 10–20 ms) produce substantial variations to performance characteristics within the inflator, but these changes are not fully transmitted to the measured external characteristics, primarily because of the choked flow condition at the nozzle exit of the inflator plenum. Finally, balanced propellant distributions, i.e., $\frac{50}{50}$, produce larger variations in output performance than do imbalanced distributions, i.e., $\frac{80}{20}$, when coupled with delay firing times between 0 and 20 ms.

Appendix: Numerical Accuracy

Based on the assumptions prescribed herein, the governing equations consist of a system of coupled ODEs that are solved by AIM using an implicit ODE solver. To determine if the proper error tolerances are used in the analysis of the dual-combustion chamber

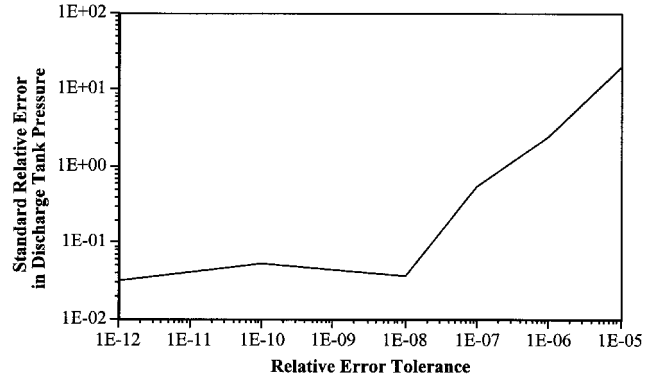

Fig. A1 Standard relative error of discharge tank pressure for varying relative error tolerances.

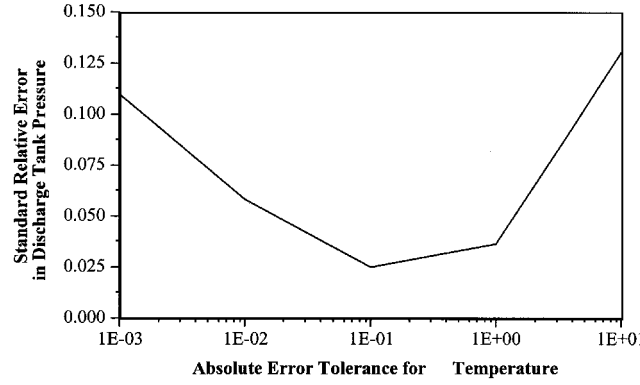

Fig. A2 Standard relative error of discharge tank pressure curve for varying absolute error tolerances for temperature.

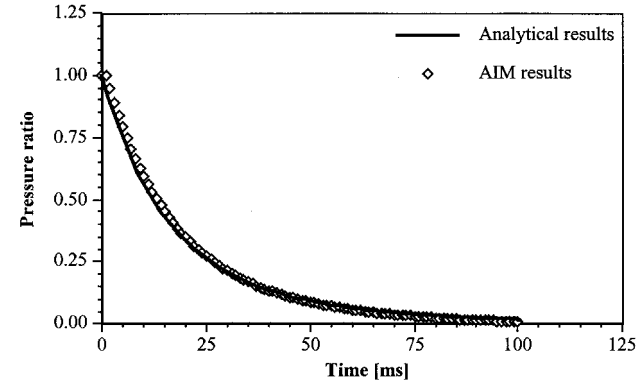

Fig. A3 Comparison of results predicted by AIM program vs an analytical solution for an isentropic discharge of a constant-volume pressurized chamber.

inflator model, a relative error calculation was used. This was performed using the standard error-of-fit error calculation

$$S_{px} = \sqrt{\left[\sum_{i=1}^{N} (p_{\mathrm{lo},i} - p_{\mathrm{hi},i})^2\right] \Big/ N} \qquad \text{(A1)}$$

where p_{lo} represents the discharge tank pressure calculated with a specified error tolerance, and p_{hi} represents the discharge tank pressure calculated when using an error tolerance one order-of-magnitude larger. Also, N represents the number of data points used as output from the simulation. Figures A1 and A2 show the relative error of the pressure curve for changing magnitudes of the relative error tolerance (RTOL) and the absolute error tolerance for temperature. For example, in Fig. A1, the standard relative error associated with a RTOL of 1×10^{-8} represents the error between calculations using RTOLs of 1×10^{-7} and 1×10^{-8}.

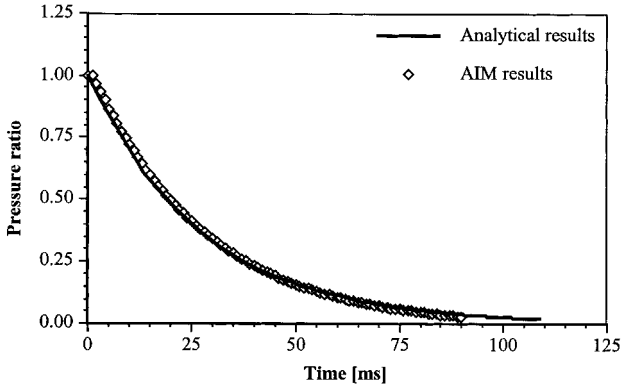

Fig. A4 Comparison of results predicted by AIM program vs an analytical solution for an isothermal discharge of a constant-volume pressurized chamber.

A blowdown simulation is used to assess the accuracy of the results provided by AIM because an exact analytical solution can be derived for this process.[15] A blowdown is when a pressurized tank of gas is depleted by exhausting through an isentropic convergent nozzle. The expression

$$t = \frac{-2V\left[(p_f/p_i)^{(1-\gamma)/2\gamma} - 1\right]}{(1-\gamma)R\sqrt{T_i}A\sqrt{(\gamma/R)[2/(\gamma+1)]^{(\gamma+1)/(\gamma-1)}}} \qquad \text{(A2)}$$

solves explicitly for the time t required to discharge a tank of volume V with gas at an initial pressure and temperature of p_i and T_i. The gas is considered to also have a constant specific heat ratio γ, and expands adiabatically. Figure A3 shows a comparison of the results from the AIM program and the analytical solution [Eq. (A2)]. The case illustrated in Fig. A2 is for the discharge of argon at an initial temperature and pressure of $T_i = 2000$ K and $P_i = 10.13$ MPa from an adiabatic tank of volume $V = 1000$ cm^3 through an isentropic discharge nozzle of area $A = 7.85 \times 10^{-5}$ m^2.

For an isothermal blowdown, where the gas within the tank is kept at a specified temperature, the expression for the time to discharge the gas within the tank is

$$t = \frac{-V}{A\sqrt{\gamma RT[2/(\gamma+1)]^{(\gamma+1)/(\gamma-1)}}}\ln\frac{p_f}{p_i} \qquad \text{(A3)}$$

Here, T is the temperature (constant) of the gas within the tank. Figure A4 shows a comparison of the results from the AIM program and the analytical solution of Eq. (A3), for the isothermal discharge of argon from the same tank when the gas temperature is held at $T = 2000$ K.

References

[1] Sutton, G. P., *Rocket Propulsion Elements*, 6th ed., Wiley, New York, 1992.

[2] Vos, T. H., and Goetz, G. W., "Inflatable Restraint Systems: Helping Save Lives on the Road," *TRW Space and Defense Quest*, Winter Issue, 1989, pp. 3–14.

[3] Berger, J. M., and Butler, P. B., "Equilibrium Analysis of Three Classes of Automotive Airbag Inflator Propellants," *Combustion Science and Technology*, Vol. 104, No. 1–3, 1995, pp. 93–114.

[4] Yang, J. C., and Grosshandler, W. L., *Solid Propellant Gas Generators: Proceedings of the 1995 Workshop*, National Institute of Standards and Technology, 5766, Gaithersburg, MD, 1995, pp. 15–18.

[5] Butler, P. B., Kang, J., and Krier, H., "Modeling and Numerical Simulation of the Internal Thermochemistry of an Automotive Airbag Inflator," *Progress in Energy and Combustion Science*, Vol. 19, No. 5, 1993, pp. 365–382.

[6] Butler, P. B., Kang, J., and Krier, H., "Modeling Pyrotechnic Combustion in an Automotive Airbag Inflator," *Europyro 93, 5th Congres International de Pyrotechnie*, Association Française de Pyrotechnie, 1993, pp. 61–70.

[7] Schmitt, R. G., Butler, P. B., and Freesmeier, J. J., "Performance and CO Production of a Non-Azide Airbag Propellant in a Pre-Pressurized Gas Generator," *Combustion Science and Technology*, Vol. 122, No. 1–6, 1997, p. 306.

[8] Butler, P. B., Kang, J., and Krier, H., "Numerical Simulation of a Pre-Pressurized Pyrotechnic Automotive Airbag Inflator," *Europyro 93, 5th Congres International de Pyrotechnie*, Association Française de Pyrotechnie, 1993, pp. 637–645.

[9] Freesmeier, J. J., "Analysis of a Dual-Combustion Chamber Gas Generator Used in Automotive Airbag Systems," M.S. Thesis, Dept. of Mechanical Engineering, Univ. of Iowa, Iowa City, IA, 1997.

[10] Butler, P. B., and Krier, H., *Airbag Inflator Model User's Guide*, Combustion Sciences, Inc., Champaign, IL, 1997.

[11] Chase, M. W., Davies, C. A., Downey, J. R., Frurip, D. J., McDonald, R. A., and Syverud, A. N., *JANAF Thermochemical Tables*, 3rd ed., American Chemical Society, New York, 1986.

[12] Cruise, D. R., "Theoretical Computations of Equilibrium Compositions, Thermodynamic Properties, and Performance Characteristics of Propellant Systems, PEP Equilibrium Code," Naval Weapons Center, TP 6037, 1973.

[13] Kuo, K. K., and Summerfield, M., *Fundamentals of Solid-Propellant Combustion*, Vol. 90, Progress in Astronautics and Aeronautics, AIAA, New York, 1984, pp. 622, 623.

[14] Zucrow, M. J., and Hoffman, J. D., *Gas Dynamics*, Vol. 1, Wiley, New York, 1976.

[15] Saad, M. A., *Compressible Fluid Flow*, Prentice–Hall, Englewood Cliffs, NJ, 1993, pp. 103–106.